Microstructure and mechanical properties of open-cell porous Ti-6Al-4V fabricated by selective laser melting

S.Y. Chen [a], J.C. Huang [a, b, *], C.T. Pan [c], C.H. Lin [c], T.L. Yang [c], Y.S. Huang [c], C.H. Ou [c], L.Y. Chen [a], D.Y. Lin [d], H.K. Lin [e], T.H. Li [f], J.S.C. Jang [f], C.C. Yang [d]

[a] Department of Materials and Optoelectronic Science, National Sun Yat-Sen University, Kaohsiung, 80424, Taiwan
[b] Institute for Advanced Study, City University of Hong Kong, Kowloon Tong, Kowloon, Hong Kong
[c] Department of Mechanical and Electro-Mechanical Engineering, National Sun Yat-Sen University, Kaohsiung, 80424, Taiwan
[d] Industrial Technology Research Institute, Hsinchu, 31040, Taiwan
[e] Graduate Institute of Materials Engineering, National Pingtung University of Science and Technology, Pingtung, 91201, Taiwan
[f] Institute of Materials Science and Engineering, National Central University, Taoyuan, 32001, Taiwan

ABSTRACT

The open-cell porous Ti-6Al-4V structure, intended to be applied as replacement for human cortical and cancellous bone, are fabricated by selective laser melting (SLM). The computer aided design (CAD) was used to design porous structures in various porosity levels from 40% to 80% and with pore sizes from 600 to 1000 μm, in order to fit the bone-tissue in-growth. The SLM porous samples with 40% to 70% porosity matched well with the CAD structure, but the 80% porosity one was found to be difficult to achieve the design. In comparison with the CAD structures and the SLM samples, there are minor discrepancies in terms of pore size and ligament width, mainly a result of laser beam broadening. To achieve more precise SLM porous morphologies, further reduction of powder size and laser beam diameter would be necessary. The measured data on the Young's modulus and yield strength of the SLM porous samples can be roughly estimated by the Gibson and Ashby model. The sample with 67% porosity was found to match best with human bone, with Young's modulus of 15 GPa and yield stress of 129 MPa, preventing from the risk of stress shielding effect.

© 2017 Elsevier B.V. All rights reserved.

1. Introduction

Additive manufacturing (AM), or termed as rapid prototyping or 3D printing, building materials directly into the final 3D shape, has become popular lately. The final products can be fabricated by adding materials layer by layer; each layer is a thin cross-section of the part derived from the original CAD data [1]. Selective laser melting (SLM) has been developed successfully for metal powders and the density of the solid part fabricated by SLM can be higher than 99% [2].

Among all pure metals and metallic alloys applied for biomedical implant, commercial-pure (CP) Ti and Ti-based alloys remain the better choices for hard tissue replacement due to their excellent mechanical, physical and biological performance [3]. In comparison

with the elastic moduli to other biocompatible alloys for implants such as Co-Cr alloy (210—253 GPa) and 316L stainless steel (190—210 GPa), the modulus of the Ti-based alloys is lower (100—140 GPa) [4], but is still much higher than the Young's modulus of human's porous tissues they replace (4—30 GPa) [5]. The higher Young's modulus of implants will make the implant basically sustain the load alone. This unwanted phenomena, so called the stress shielding effect, will lead to bone osteoporosis [6].

In order to further reduce and match the modulus of the Ti-based parts with human bones, applying porous structures could be a solution. There have been some natural porous materials, such as Zeolite, activated carbon and spongy bone. Porous materials are well known to possess unique characteristics such as low density, high-surface-area ratio and high mechanical energy absorption efficiency [7]. In order to promote human tissues to grow into the pores, the desired micro-pore size in the porous implant metals needs to be controlled at the scale about 300—800 μm, according to previous studies and review papers [8—13]. Some previous studies have demonstrated that the nano-structured surface morphology

of the implant is an important property for osseointegration [14–17]. Nano-structured surface morphology is favorable for cell attaching on the surface, but not really for the whole bone-cell ingrowth. The normal bone cells, typically several micrometers in size, would be much larger than the nano-structured pores. Therefore, in this study, the open-cell pore sizes with micrometer range are designed, beneficial to the whole bone-cell ingrowth. Usually, pore sizes more than 300 μm are recommended, due to enhanced new bone formation and the formation of capillaries. Because of vascularization, pore size has been shown to affect the progression of osteogenesis. Small pores would favor the hypoxic conditions and would induce osteochondral formation before osteogenesis; while large pores, that are well-vascularized, would lead to direct osteogenesis (without preceding cartilage formation).

In some previous efforts, porous metallic foams have been fabricated by powder metallurgy by mixing metallic and salt powders [18–20]. In this study, SLM is adopted to prepare similar metallic porous structures. The resulting microstructure and mechanical properties are reported.

2. Materials and methods

The starting Ti-6Al-4V powders (Titanium Ti64ELI) were purchased from EOS, Germany. SLM was conducted by an EOSINT M 280 AM machine also from EOS, Germany. The 3D-printing specimens were built under an Ar protective atmosphere, with a setting power of 190 W, scanning speed of 1200 mm/s, beam diameter of 70 μm, and single layer thickness of 30 μm. The open-cell porous sample models with different porosity levels and random micro pore sizes from 500 to 800 μm, as shown in Fig. 1, were designed using the SolidWorks CAD software (SolidWorks, USA). The general porosity of the porous structures, ε, was calculated by formula [21]

$$\varepsilon = \left(1 - \frac{\rho}{\rho_s}\right) \times 100, \tag{1}$$

where ρ and ρ_s are the density of the porous structure and its theoretical density of solid part. The density of the porous structure was measured from its weight and dimensional measurements. The theoretical density of solid part is 4.37 g cm^{-3} for the Ti-6Al-4V alloys.

The structure of powders and porous specimens were characterized by X-ray diffraction (SIEMENS D5000 X-ray diffractometer (XRD), using the Cu-Kα radiation with its wavelength of 1.5406 A). The operating parameters of XRD were 40 kV and 30 mA, and equipped with 0.02 mm graphite monochromator. The scanning range of diffraction angle was from 20° to 80°, with a scanning rate of 0.05° per 4 s. In addition, these pre-SLM powders and porous structures were examined by scanning electron microscopy (SEM, JEOL JSM-6330), combined with the quantitative ImageJ software image analysis, in order to characterize the powder distribution and pore size.

Cylindrical porous samples for compression tests, with a diameter of 10 mm and a height of 6 mm, were used to extract their mechanical properties. The samples are tested at a strain rate of 1×10^{-4} s^{-1} at room temperature by using the Instron 5582 universal testing machine, equipped with the Instron 2601 Linear Variable Differential Transformer (LVDT) displacement transducer.

The data on the elastic modulus and yield stress of all porous Ti-based samples were compared with the predicted values based on the Gibson and Ashby model [22]. According to this model, the mechanical properties are related to the porosity (or the relative density) of open-cell porous structures. The relationships between elastic modulus, plateau stress and relative density are given by

$$E/E_s = C_1(\rho/\rho_s)^{n_1} \tag{2}$$

$$\sigma_{pl}/\sigma_s = C_2(\rho/\rho_s)^{n_2}, \tag{3}$$

where E is the elastic modulus of the porous structure, E_s is the elastic modulus of the open-cell edge (ligament) material, σ_{pl} is the plateau stress of the porous material, σ_s is the yield strength of the ligament material, ρ is the porous structure density, ρ_s is the density of the ligament material, and C_1, C_2, n_1 and n_2 are constants depending on the porous structure. The elastic modulus (E_s) and yield strength (σ_s) of dense Ti-6Al-4V alloys fabricated by SLM are 110 GPa and 990 MPa [23]. According to previous studies fitting many experimental data [19,24], n_1 is a constant of around 2 and n_2 is a constant of around 1.5 for open-cell porous structures. Furthermore, the complex dependence of the C_1 and C_2 constants
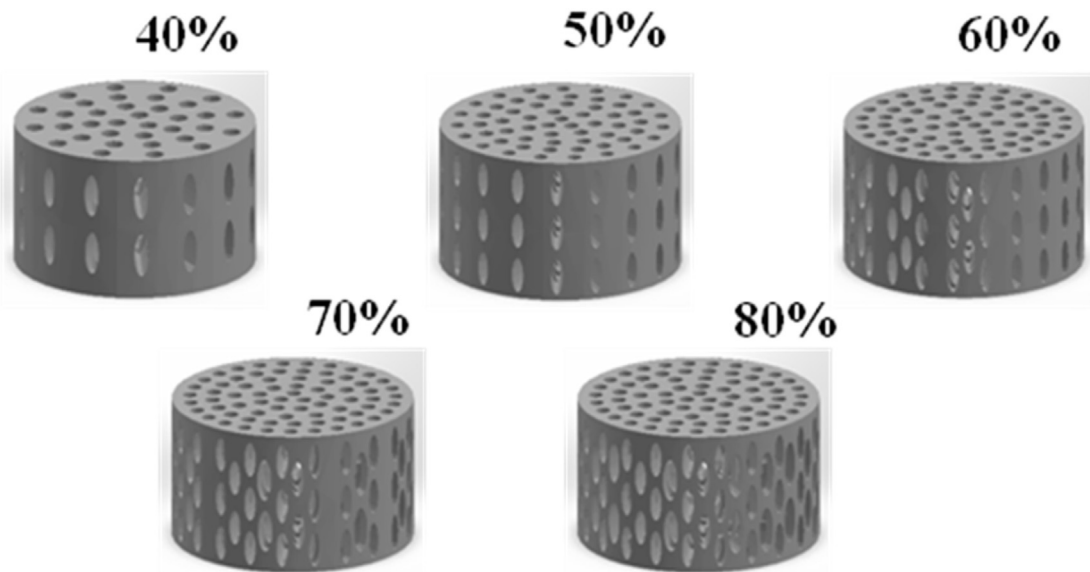

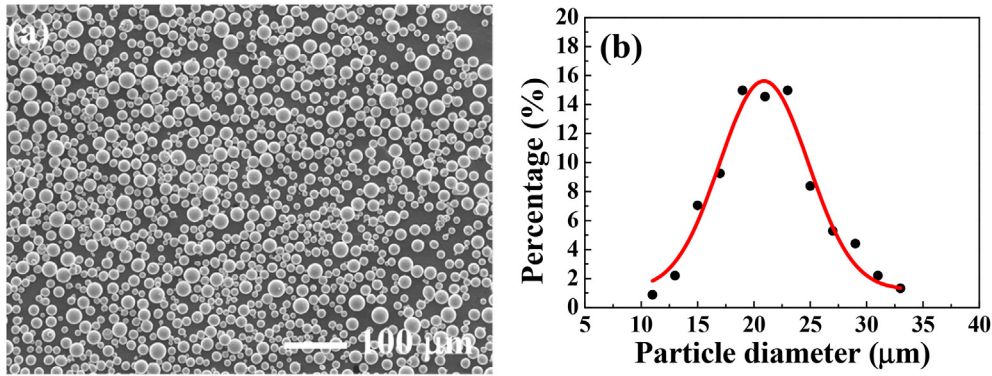**Fig. 1.** The CAD data with different porosity levels.

Fig. 2. (a) The SEM morphology and (b) the size distribution of Ti-6A1-V pre-alloyed powders.
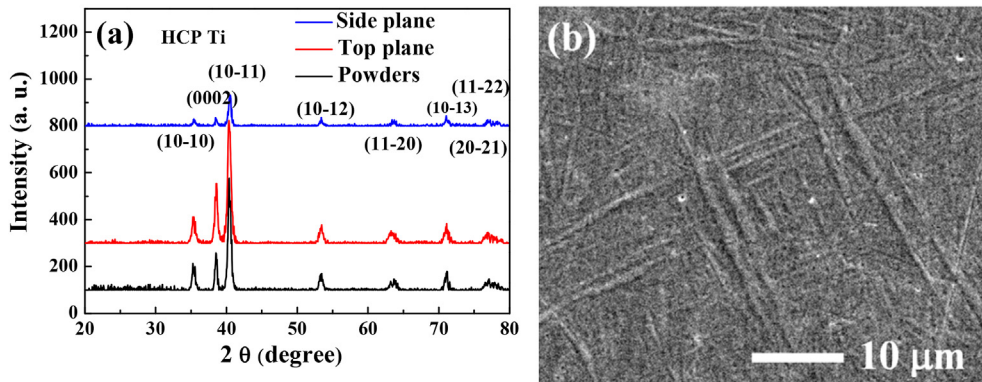

Fig. 3. XRD patterns of the as-built porous Ti-6Al-4V specimen side plane, top plane, and the Ti-6A1-4V pre-SLM powders. Basically, there texture can be considered to be rather random, with minimum preferred packing orientation. (b) A representative SEM micrograph taken from the SLM 67% structure sample, showing the typical fine needle α′ martensite morphology.

for porous structures is related to the bonding strength of the cell ligaments, mostly varying in the range of 0.1—4.0 [25].

3. Results and discussion

The as-received Ti-6Al-4V pre-SLM powders appear to possess the smooth, spherical, and fully dense surface appearance, sometimes with a few satellites, as shown in Fig. 2(a). Based on the measurements from about 200 powders using the ImageJ software image analysis, a near Gaussian (i.e. normal) distribution with an average particle size about 20.6 ± 4.6 µm can be seen from Fig. 2(b). Note that the highly spherical shape (with the ratio of the long

versus short axis about 0.962 ± 0.009) of the powders is favorable for subsequent SLM processes [26].

The commercial Ti-6Al-4V alloys can possess the hexagonal closed packing (HCP) α-Ti phase and the body-centered cubic (BCC) β-Ti phase. The transformation temperature of β-Ti phase was about 980 °C [27]. The β-Ti phase can be clearly characterized by the (110) and (200) reflections, with $2\theta = 39.5°$ and $2\theta = 57°$ in XRD patterns [28]. Different heat treatment temperatures and cooling rates could control the specific phase to be formed. According to those XRD patterns presented in Fig. 3, β-Ti phase is hardly detected. If there is any β phase, the amount should be very low. It is clear from Fig. 3 that the as-received Ti-6Al-4V powders are composed
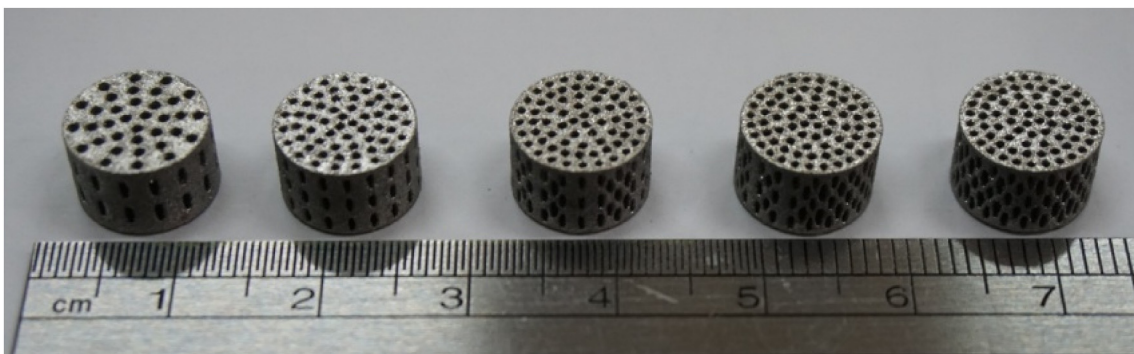

Fig. 4. The Ti-6Al-4V porous specimens fabricated by SLM. The porosity levels from left to right are 43%, 49%, 60%, 67% and 71%.

Table 1
Summary of mechanical properties of the Ti-6Al-4V structures fabricated by SLM with different designed CAD models.

Designed porosity (%)	Real porosity (%)	Young's modulus (GPa)	Yield stress (MPa)	ρ/ρ_s	E/E_s	σ/σ_s	$(\rho/\rho_s)^2$	$(\rho/\rho_s)^{1.5}$
40	43 ± 0.4	55.0 ± 2.4	564.7 ± 3.1	0.572	0.499	0.570	0.327	0.433
50	49 ± 0.9	44.4 ± 1.3	465.4 ± 2.1	0.514	0.404	0.470	0.264	0.369
60	60 ± 0.4	24.4 ± 1.0	233.9 ± 3.4	0.404	0.222	0.236	0.163	0.257
70	67 ± 0.4	15.3 ± 1.4	128.7 ± 5.6	0.331	0.139	0.130	0.110	0.190
80	71 ± 0.1	9.7 ± 1.9	62.0 ± 7.9	0.297	0.088	0.063	0.088	0.162

Table 2
Summary of the pore size and ligament width of the Ti-6Al-4V porous structures fabricated by SLM with different designed CAD models. The difference between the designed and measured pore size and ligament width is seen to increase from about 2–6% for low porosity samples up to about 8–16% for high porosity samples. Note that the pore size data measured from the side views for those elongated pores are in fact referred to the circle diameter of the equivalent cross-sectional area.

| Designed/measured porosity (%)	Designed/measured pore size (μm)		Designed/measured ligament width (μm)	
	Top views	Side views	Top views	Side views
40/43 ± 0.4	777 ± 4/749 ± 19	1014 ± 5/964 ± 20	783 ± 414/833 ± 448	1090 ± 427/1110 ± 315
50/49 ± 0.9	611 ± 6/559 ± 35	841 ± 2/787 ± 25	540 ± 137/591 ± 160	806 ± 365/857 ± 281
60/60 ± 0.4	641 ± 4/589 ± 33	855 ± 4/799 ± 68	455 ± 135/488 ± 152	480 ± 226/506 ± 238
70/67 ± 0.4	611 ± 2/564 ± 37	820 ± 12/783 ± 68	425 ± 130/461 ± 126	420 ± 209/459 ± 240
80/71 ± 0.1	666 ± 2/559 ± 52	847 ± 9/786 ± 39	369 ± 77/427 ± 89	348 ± 181/396 ± 204
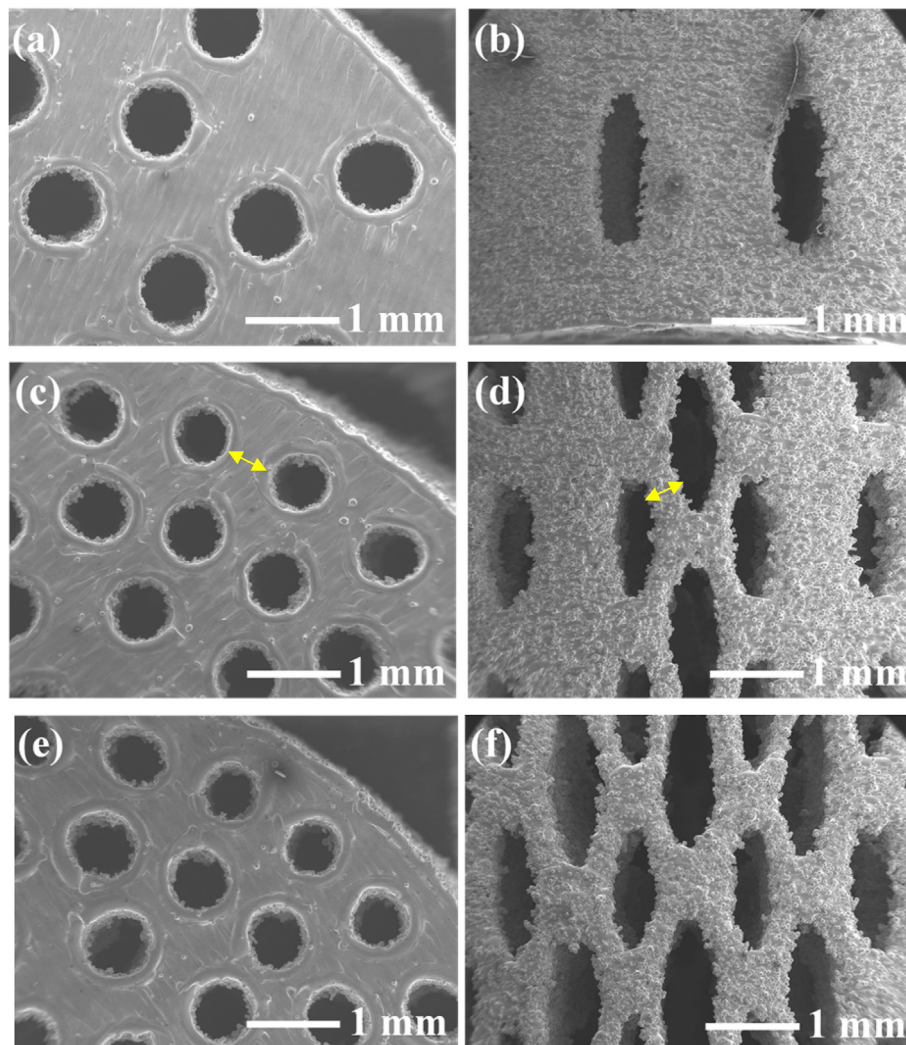
Fig. 5. Representative SEM micrographs taken from the top planes (left images, (a), (c) and (e)) and from the side planes (right images, (b), (d) and (f)) of the porous Ti-6Al-4V structures fabricated by SLM, with the measured porosity of (a) and (b) 43%, (c) and (d) 60%, and (e) and (f) 71%.
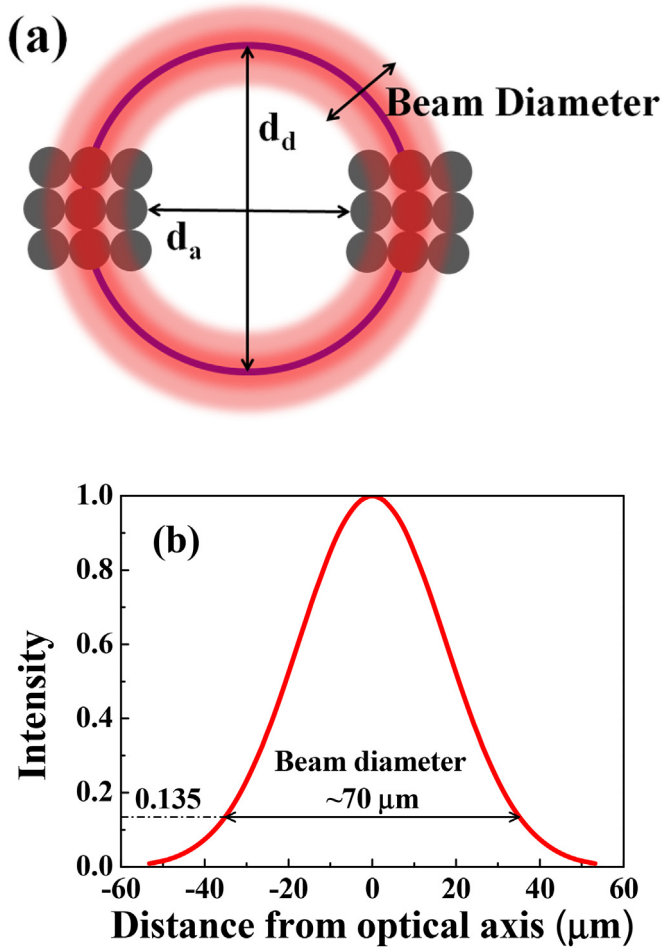
Fig. 6. (a) Schematic drawing showing the CAD designed pore size with a dimension of d_d, and the actual SLM printed pore size with a dimension of d_a; d_a is always smaller than d_d by about 50 μm. The discrepancy is due to the laser beam broadening with a finite beam size and a Gaussian intensity distribution. The Ti-6Al-4V powders could attach the pore edge during SLM, making actual pore size smaller. (b) The Gaussian intensity distribution of the laser beam applied.

predominantly of the HCP phase. The current HCP structure of the powders is similar to what Simonelli et al. [29] have reported. Fig. 3(a) also shows both XRD patterns obtained from the top and side planes of the SLM porous samples. Basically, there is no apparent difference between these top and side patterns, revealing the uniform orientation with minimum preferred texture. Meanwhile, the XRD patterns of the SLM porous samples are similar to that of the as-received powders. The high cooling rate occurring during the SLM process retained the random uniform texture of the powders. Nevertheless, the measured XRD patterns in Fig. 3 can be attributed to both the stable α-phase and the metastable α′ martensite, as they have the same crystalline structure and very similar lattice parameters [30]. From the SEM micrograph presented in Fig. 3(b), most of the microstructure in the SLM structure samples can be interpreted as the α′ martensite phase with the typical fine needle morphology [31,32].

Fig. 4 shows the different porous samples fabricated by SLM according to different CAD data. The different porous samples are all open-cell, in agreement with the CAD design, and the ratio of the measured density to the fully dense Ti-6Al-4V is in the range 0.297–0.572, as listed in Table 1. The 3D-fabricated Ti-6Al-4V porous specimens in Fig. 4 exhibit the measured porosity volume fractions, based on Equation (1), of 43% ± 0.4%, 49% ± 0.9%,

60% ± 0.4%, 67% ± 0.4% and 71% ± 0.1%, respectively. The measured porosity is similar to the CAD designed porosity in the range of 40–70%. However, it is difficult to achieve the highest designed porosity 80% by the current SLM; the resulting porosity for this case is in fact about 71%. This is because that the designed porosity values were determined by CAD calculation data, and the CAD-designed model uses all smooth surfaces for the pore surfaces. But, the real sample surfaces fabricated by 3D printing were not similar to the CAD-designed smooth surfaces. The effect of rougher pore surface becomes significant for the highest-porosity (80%) samples. For this porous sample with the highest designed porosity (80%, or the real porosity of 71%), the real ligament widths achieved by 3D printing (i.e., 427 and 396 μm) could not reach the level designed by CAD (i.e., 369 and 348 μm), as presented in Table 2. It follows that the real porosity would be lower than the designed porosity.

Fig. 5 shows some representative SEM micrographs, taken from the top and side views of the SLM porous samples. The pore number density appears to increases with increasing porosity. In consistent with the CAD design, the resulting pores seen from the top plane (or any horizontal cross-sectional cut) are basically circular, while the pores viewed from the side plane are elongated. Such an elongated pore shape was intentionally designed to achieve higher compressive strength along the vertical direction. The data obtained from careful measurements on the pore sizes (measured from the top and side views), as well as the ligament width (defined in Fig. 5(c) and (d) by arrows, also measured from the top and side views) are all complied in Table 2. It can be seen from Table 2 that the average pore size mostly varies from 600 to 900 μm, and is not strongly related to the porosity level. These pore sizes are compatible to the designed sizes, and are large enough for human bone tissues to grow in Refs. [33–35]. From the CAD data and porous parts, the numbers of pores in the top plane or side plane both increase with increasing porosity, and the ligament widths decrease with increasing porosity.

From Table 2, there are several other trends that can be noted. (i) The experimentally measured pore sizes are always smaller than the designed pore sizes, and the experimentally measured ligament width data are always higher than the designed width values, meaning that the Ti-4Al-4V powders (partially melted by laser) tend to occupy more space near the pore boundaries than what are designed by CAD, due to the finite laser beam width (not point source) with a Gaussian distribution. (ii) The mismatch of the pore size and ligament width for the designed 40–70% porosity samples is less than 10%, revealing that the current SLM experiments can successfully reproduce the structures predicted by CAD. Only the designed 80% porosity sample shows a mismatch about 10–16%. (iii) The difference between the CAD designed and the experimentally measured values for both the pore size and ligament width appears to increase with increasing porosity level, being about 2–6% for the low porosity samples and about 8–16% for the high porosity samples, still a result of the Gaussian distributed laser beam energy. (iv) The pore size variation over these five samples is not significant, all about 600–800 μm measured from the top view and about 850–1000 μm from the side view. The increase of porosity is basically a result of the increase of pore numbers due to the decrease of ligament width under the same volume, the latter decreasing from about 800 μm (top view) or 1100 μm (side view) for the 40% porosity sample down to about 370 μm (top view) or 350 μm (side view) for the 80% one.

Attempts have been made to figure out the main cause for the discrepancy (2–16%) between the CAD design and SLM printing. From the raw data in Table 2, it can be found that although the difference percentage increases with increasing porosity level (2% up to 16%), all of the raw mismatch values for the SLM-fabricated
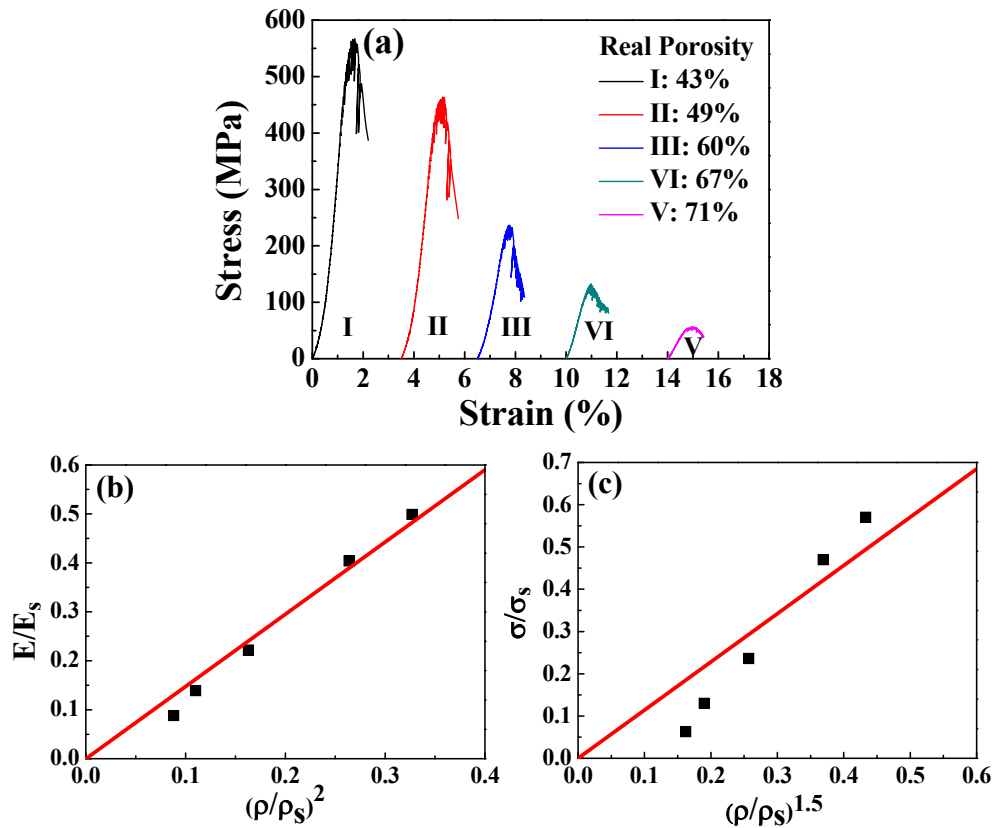
Fig. 7. (a) Compressive stress-strain curves for the Ti-6Al-4V structure specimens fabricated by SLM with various porosity levels from 43% to 71%. Based on the Gibson and Ashby equation, it shows the dependence of the elastic modulus and yield stress as function of the relative Ti-6A1-4V density. The fitting R^2 for (b) is 0.992 and for (c) is 0.932.

samples with actual porosity from 43% to 71% are in fact all scattered within −50 μm for the pore size and scattered within +50 μm for the ligament width. Since the Ti-6Al-4V powders used in the current SLM process measure 20.6 ± 4.6 μm in diameter, the −50 μm or +50 μm discrepancies should be a result of the over-occupancy of the powders during SLM. Fig. 6(a) is a schematic drawing for the likely happening. The laser beam size applied in SLM is about 70 μm, with a typical Gaussian intensity distribution (Fig. 6(b)), possessing the strongest intensity at the center and attenuating toward both ends. The central region with stronger beam intensity is estimated to be about 30 μm. Within this 30 μm, the Ti-6Al-4V powders would be melted and attached to the pore edges. This laser beam broadening and laser melting edge effects would make more powders attach to the pore edges, and would in-turn result in the smaller pore sizes and larger ligament width. If we need to improve and produce more precise SLM pores or other morphologies, the powder size and the laser beam size both need to be narrowed down.

The compressive stress-strain curves of porous Ti-6Al-4V SLM samples with different actual porosity levels in the range of 43%–71% are shown in Fig. 7(a). Both Young's modulus and yield stress decrease with increasing real porosity level. The calculated Young's moduli and yield stresses are also listed in Table 1. For porous Ti-6Al-4V scaffolds, as the porosity raises from 43% to 71%, the Young's modulus decreases from 55.8 to 7.8 GPa and the yield stress decreases from 565 to 62 MPa. Worth speaking, the porous Ti-6Al-4V SLM sample with 67% actual porosity, showing a Young's modulus of 15 GPa and a yield stress of 129 MPa, is similar to human bone in terms of mechanical properties [36]. The porous Ti-6Al-4V SLM sample with an actual porosity of 67% presents the

Young's modulus and yield stress of about 15 GPa and 129 MPa, which are similar to the mechanical properties of human bone [36]. Compared with the typical range of Young's modulus and yield strength of human cortical bone and cancellous bone of 4–30 GPa and 20–193 MPa [3,5], the mechanical properties of the current SLM porous Ti-6Al-4V samples offer highly compatible characteristics which can avoid the risk of stress shielding effect.

Following the Gibson and Ashby model, the calculated data are all listed in Table 1. Fig. 7(b) and (c) are the plots based on Equations (2) and (3), presenting the variation of normalized elastic modulus (E/E_s) and yield stress (σ/σ_s) of the porous Ti-6Al-4V samples. It can be seen that the Young's modulus data are better predicted by the Gibson-Ashby model in the whole range of relative density. The fitting line for the elastic modulus gives the relationship $E/E_s = 1.5(\rho/\rho_s)^2$, with a high fitting R^2 value of 0.992. The fitting line for the yield stress gives the relationship $\sigma/\sigma_s = 1.1(\rho/\rho_s)^{1.5}$, with the fitting R^2 value of 0.932. Note that the intentional fitting line in Fig. 7(b) for the yield stress shows deviation from the data; those data on the lower density (or higher porosity) cases tend to fall below the fit line predicted by the model. This suggests that the bonding conditions for the samples with lower density (or higher porosity) were not as strong as those with higher density (or lower porosity), leading to lower yield stresses for smaller $(\rho/\rho_s)^2$ values. In the Gibson and Ashby model, the C_1 and C_2 proportional coefficients have been experimentally reported to vary mostly within 1–4 and 0.1–1 for open-cell structures [25], depending on the bonding strength of the cell ligaments. The dependence of elastic modulus can be roughly predicted by this model, but the dependence of yield stress is only fair. Nevertheless, the current C_1 and C_2 values of ~1.5 and 1.1 for the SLM porous samples are already higher

than the values in our previous studies, $C_1 = 0.8$ and $C_2 = 0.4$, using the traditional powder metallurgy method [19]. This result implies that the current porous SLM products already have sufficient bonding strength than the porous structures fabricated by traditional space holder method.

4. Conclusions

The porous Ti-6Al-4V structures, intended to apply as replacement of human cortical bone and cancellous bone, are successfully fabricated by selective laser melting (SLM). The following conclusion can be drawn.

(1) The CAD designed structures contain various porosity levels in the range from 40% to 80%, with pore sizes from 600 to 1000 μm, suitable for bone tissue in-growth. The SLM structure samples with 40% to 70% porosity match well with their original CAD designs; nevertheless, the sample with CAD designed 80% porosity is difficult to achieve.
(2) The difference between the CAD designed and experimentally measured values for both pore size and ligament width appears to increase with increasing porosity level. The difference is about 2–6% for the low porosity samples and about 8–16% for the high porosity samples.
(3) The discrepancy between CAD and SLM pore size and ligament width is mainly caused by the laser beam broadening. If we need to improve and produce more precise SLM pores or other morphologies, the powder size and the laser beam size both need to be narrowed down.
(4) The SLM structure samples all possess basically HCP α or α′ phase, with minimum BCC β phase.
(5) The Young's modulus data on the porous Ti-6Al-4V scaffolds decrease from 55.8 to 7.8 GPa, and the yield stress data decrease from 565 to 62 MPa as the porosity raises from 43% to 71%. The sample with 67% actual porosity presents a Young's modulus of 15 GPa and a yield stress of 129 MPa, matched well with the mechanical properties of human bone, avoiding the risk of stress shielding effect.
(6) The measured Young's modulus and yield strength of the SLM structure samples can be roughly predicted by the Gibson and Ashby model.

Acknowledgments

References

[1] I. Gibson, D.W. Rosen, B. Stucker, Additive Manufacturing Technologies, Springer, 2010.
[2] B. Vandenbroucke, J.P. Kruth, Selective laser melting of biocompatible metals for rapid manufacturing of medical parts, Rapid Prototyp. J. 13 (2007) 196–203.
[3] Y. Li, C. Yang, H. Zhao, S. Qu, X. Li, Y. Li, New developments of Ti-based alloys for biomedical applications, Materials 7 (2014) 1709–1800.
[4] M. Geetha, A.K. Singh, R. Asokamani, A.K. Gogia, Ti based biomaterials, the ultimate choice for orthopaedic implants – a review, Prog. Mater. Sci. 54 (2009) 397–425.
[5] P.K. Zysset, X. Edward Guo, C. Edward Hoffler, K.E. Moore, S.A. Goldstein, Elastic modulus and hardness of cortical and trabecular bone lamellae measured by nanoindentation in the human femur, J. Biomech. 32 (1999) 1005–1012.
[6] R. Huiskes, Stress shielding and bone resorption in THA: clinical versus computer-simulation studies, Acta Orthop. Belg. 59 (1993) 118–129.
[7] M.E. Davis, Ordered porous materials for emerging applications, Nature 417 (2002) 813–821.
[8] A.J.T. Clemow, A.M. Weinstein, J.J. Klawitter, J. Koeneman, J. Anderson, Interface mechanics of porous titanium implants, J. Biomed. Mater. Res. 15 (1981) 73–82.
[9] L. Zhang, Y.Q. Zhang, Y.H. Jiang, R. Zhou, Superelastic behaviors of biomedical porous NiTi alloy with high porosity and large pore size prepared by spark plasma sintering, J. Alloys Compd. 644 (2015) 513–522.
[10] J. Wegrzyn, K.R. Kaufman, A.D. Hanssen, D.G. Lewallen, Performance of porous tantalum vs. titanium cup in total hip arthroplasty: randomized trial with minimum 10-year follow-up, J. Arthroplasty 30 (2015) 1008–1013.
[11] J.D. Bobyn, G.J. Stackpool, S.A. Hacking, M. Tanzer, J.J. Krygier, Characteristics of bone ingrowth and interface mechanics of a new porous tantalum biomaterial, J. Bone Jt. Surg. 81B (1999) 907–914.
[12] V. Karageorgiou, D. Kaplan, Porosity of 3D biomaterial scaffolds and osteogenesis, Biomaterials 26 (2005) 5474–5491.
[13] G. Hannink, J.J. Chris Arts, Bioresorbability, porosity and mechanical strength of bone substitutes: what is optimal for bone regeneration? Inj. Int. J. Care Inj. 42 (2011) S22–S25.
[14] G. Zhao, Z. Schwartz, M. Wieland, F. Rupp, J. Geis-Gerstorfer, D.L. Cochran, High surface energy enhances cell response to titanium substrate microstructure, J. Biomed. Mater. Res. A 74 (2005) 49–58.
[15] L. Wang, G. Zhao, R. Olivares-Navarrete, B.F. Bell, M. Wieland, D.L. Cochran, Integrin beta1 silencing in osteoblasts alters substrate-dependent responses to 1,25-dihydroxy vitamin D3, Biomaterials 27 (2006) 3716–3725.
[16] G. Zhao, O. Zinger, Z. Schwartz, M. Wieland, D. Landolt, B.D. Boyan, Osteoblastlike cells are sensitive to submicron-scale surface structure, Clin. Oral Implants Res. 17 (2006) 258–264.
[17] G. Mendonça, D.B.S. Mendonça, F.J.L. Aragao, L.F. Cooper, Advancing dental implant surface technology – from micronto nanotopography, Biomaterials 29 (2008) 3822–3835.
[18] T. Aydogmus, S. Bor, Processing of porous TiNi alloys using magnesium as space holder, J. Alloys Compd. 478 (2009) 705–710.
[19] J.B. Li, H.C. Lin, J.S.C. Jang, C.N. Kuo, J.C. Huang, Novel open-cell bulk metallic glass foams with promising characteristics, Mater. Lett. 105 (2013) 140–143.
[20] X. Zhang, H. Hou, L. Wei, Z. Chen, W. Wei, L. Geng, High damping capacity in porous NiTi alloy with bimodal pore architecture, J. Alloys Compd. 550 (2013) 297–301.
[21] V. Weißmann, R. Bader, H. Hansmann, N. Laufer, Influence of the structural orientation on the mechanical properties of selective laser melted Ti6Al4V open-porous scaffolds, Mater. Des. 95 (2016) 188–197.
[22] L.J. Gibson, M.F. Ashby, The mechanics of three-dimensional cellular materials, Proc. R. Soc. Lond. A 382 (1982) 43–59.
[23] L. Facchini, E. Magalini, P. Robotti, A. Molinari, S. Höges, K. Wissenbach, Ductility of a Ti-6Al-4V alloy produced by selective laser melting of prealloyed powders, Rapid Prototyp. J. 16 (2010) 450–459.
[24] T.Y. Wu, X. Wang, J.C. Huang, W.Y. Tsai, Y.Y. Chu, S.Y. Chen, X.H. Du, Characterization and functional applications of nanoporous Ag foams prepared by chemical dealloying, Metall. Mater. Trans. B 46 (2015) 2296–2304.
[25] M. Ashby, A. Evans, N. Fleck, L. Gibson, J. Hutchinson, H. Wadley, Metal Foams: a Design Guide, Butter.-Heinemann, Oxford, 2000.
[26] M.W. Wu, P.H. Lai, The positive effect of hot isostatic pressing on improving the anisotropies of bending and impact properties in selective laser melted Ti-6Al-4V alloy, Mater. Sci. Eng. A 658 (2016) 429–438.
[27] M.T. Jovanović, S. Tadić, S. Zec, Z. Mišković, I. Bobić, The effect of annealing temperatures and cooling rates on microstructure and mechanical properties of investment cast Ti–6Al–4V alloy, Mater. Des. 27 (2006) 192–199.
[28] S.L.R. da Silva, L.O. Kerber, L. Amaral, C.A. dos Santos, X-ray diffraction measurements of plasma-nitrided Ti–6Al–4V, Surf. Coat. Technol. 116–119 (1999) 342–346.
[29] M. Simonelli, Y.Y. Tse, C. Tuck, The formation of α+β microstructure in as-fabricated selective laser melting of Ti–6Al–4V, J. Mater. Res. 29 (2014) 2028–2035.
[30] Y. Zhou, S.F. Wen, B. Song, X. Zhou, Q. Teng, Q.S. Wei, Y.S. Shi, A novel titanium alloy manufactured by selective laser melting: microstructure, high temperature oxidation resistance, Mater. Des. 89 (2016) 1199–1204.
[31] I. Yadroitsev, P. Krakhmalev, I. Yadroitsava, Selective laser melting of Ti6Al4V alloy for biomedical applications: temperature monitoring and microstructural evolution, J. Alloys Compd. 583 (2014) 404–409.
[32] H. Attar, M. Calin, L.C. Zhang, S. Scudino, J. Eckert, Manufacture by selective laser melting and mechanical behavior of commercially pure titanium, Mater. Sci. Eng. A 593 (2014) 170–177.
[33] E. Tsuruga, H. Takita, H. Itoh, Y. Wakisaka, Y. Kuboki, Pore size of porous hydroxyapatite as the cell-substratum controls BMP-induced osteogenesis, J. Biochem. 121 (1997) 317–324.
[34] C.M. Murphy, M.G. Haugh, F.J. O'Brien, The effect of mean pore size on cell attachment, proliferation and migration in collagen–glycosaminoglycan scaffolds for bone tissue engineering, Biomaterials 31 (2010) 461–466.
[35] S. Ahmadi, S.K. Sadrnezhaad, A novel method for production of foamy core@ compact shell Ti6Al4V bone-like composite, J. Alloys Compd. 656 (2016) 416–422.
[36] X.J. Wang, Y.C. Li, P.D. Hodgson, C.E. Wen, Nano-and macro-scale characterisation of the mechanical properties of bovine bone, Mater. Forum 31 (2007) 156–159.